

Atomistic modeling of the channeling process with and without account for ionising collisions: A comparative study

Gennady B. Sushko,¹ Andrei V. Korol,^{1,*} and Andrey V. Solov'yov^{1,†}

¹*MBN Research Center, Altenhöferallee 3, 60438 Frankfurt am Main, Germany*

This paper presents a quantitative analysis of the impact of inelastic collisions of ultra-relativistic electrons and positrons, passing through oriented crystalline targets, on the channeling efficiency and on the intensity of the channeling radiation. The analysis is based on the numerical simulations of the channeling process performed using the MBN EXPLORER software package. The ionising collisions, being random, fast and local events, are incorporated into the classical molecular dynamics framework according to their probabilities. This methodology is outlined in the paper. The case studies presented refer to electrons with energy ε ranging from 270 to 1500 MeV and positrons with $\varepsilon = 530$ MeV incident on thick (up to 1 mm) single diamond, silicon and germanium crystals oriented along the (110) and (111) planar directions. In order to elucidate the role of the ionising collisions, the simulations were performed with and without account for the ionising collisions. The case studies presented demonstrate that both approaches yield highly similar results for the electrons. For the positrons, the ionising collisions reduce significantly the channeling efficiency. However, it has been observed that this effect does not result in a corresponding change in the radiation intensity.

I. INTRODUCTION

Interaction of high-energy charged particles with crystals is sensitive to the orientation of the incoming beam with respect to the main crystallographic directions (planar and axial) of the target. Projectiles, incident at small angles to the crystal planes (or axes) experience specific channeling motion following the planar (axial) direction experiencing collective action of the electrostatic fields of the lattice atoms [1].

* korol@mbnexplorer.com

† solovyov@mbnresearch.com

The study of the channeling process of ultra-relativistic particles in oriented crystals has emerged as a wide-ranging field of research [2–5]. Various applications have been suggested including beam steering [6–8], collimation [9], focusing [10], and extraction [2].

Oriented crystals of different geometries (single, bent, periodically bent) exposed to the beams of ultra-relativistic electrons and positrons can potentially serve as novel intensive gamma-ray crystal-based light sources (CLS) operating in the MeV-GeV photon energy range [5, 11, 12]. Practical realization of CLSs is a subject of the running Horizon Europe EIC-Pathfinder-2021 project TECHNO-CLS [13]. This Project presents a high-risk/high-gain science-towards-technology breakthrough research aimed at further development of technologies for crystal samples preparation, extensive experimental program that includes design and manipulation of particle beams, detection and characterization of the radiation, as well as theoretical analysis and advanced computational modelling for the characterisation of CLS.

In recent years, advanced atomistic computational modeling of the channeling process and the process of the photon emission as well as of other related phenomena beyond the continuous potential framework has been carried out using the multi-purpose computer package MBN EXPLORER [14, 15] and the special multi-task software toolkit with graphical user interface MBN STUDIO [16]. The computation accounts for the interaction of projectiles with separate atoms of the environments, whereas many different interatomic potentials implemented in MBN EXPLORER support rigorous simulations of various media [17, 18]. For simulations of the channeling and related phenomena, an additional module has been incorporated into MBN EXPLORER to compute the motion of relativistic projectiles along with dynamical simulations of the environments. This methodology, called relativistic molecular dynamics (MD), has been extensively applied to simulate passage of ultra-relativistic charged particles in oriented crystals accompanied by emission of intensive radiation. A comprehensive description of the multiscale all-atom relativistic MD approach as well as a number of case studies related to modeling channeling and photon emission by ultra-relativistic projectiles are presented in a review article [19].

The aim of the present study is to quantify the impact of the ionising collisions on the channeling efficiency and on the photon emission spectra for projectile particles of different charge and energy passing through comparatively thick crystalline targets. For doing this we have followed general methodology implemented in MBN EXPLORER to generate parti-

cles' trajectories in a crystalline environment that accounts for randomness in sampling the incoming projectiles as well as in displacement of the lattice atoms from the nodal positions due to thermal vibrations. As a result, each trajectory corresponds to a unique crystalline environment. Another phenomenon that contributes to the statistical independence of the simulated trajectories, concerns the events of inelastic scattering of a projectile particle from the crystal atoms resulting in the excitation or ionisation of the atom. These collisions lead to a random change in the direction of the particle's velocity, which in turn leads to a change in its transverse energy. These quantum events are random and occur on the atomic scale in terms of time and space, therefore they can be incorporated into the classical mechanics framework in accordance with their probabilities.

The methodology implemented in MBN EXPLORER to account for the ionising collisions is discussed in Section II. In Section III we present and discuss the results of simulations of the channeling process of the sub-GeV electrons and positrons in different crystalline targets. A summary of the results obtained is given in Section IV.

II. METHODOLOGY

The MBN EXPLORER package [14, 17] implements the method of relativistic classical MD [15] to model the motion an ultra-relativistic particle in an external field or/and in an atomic environment. The code integrates the relativistic equations of motion of a particle of mass m , charge q and energy ε written in the following form (see, e.g., [20]):

$$\begin{cases} \dot{\mathbf{v}} = \frac{\mathbf{F} - \boldsymbol{\beta}(\mathbf{F} \cdot \boldsymbol{\beta})}{m\gamma} \\ \dot{\mathbf{r}} = \mathbf{v} \end{cases}, \quad (1)$$

where $\mathbf{r} = \mathbf{r}(t)$ and $\mathbf{v} = \mathbf{v}(t)$ are instantaneous position vector and velocity of the particle, $\boldsymbol{\beta} = \mathbf{v}/c$, $\gamma = \varepsilon/mc^2$ is the Lorentz factor, and c is the speed of light.

In a general case, the force \mathbf{F} acting on the projectile is the sum of two terms:

$$\mathbf{F} = \mathbf{F}_{\text{em}} + \mathbf{F}_{\text{rd}}. \quad (2)$$

Here \mathbf{F}_{em} denotes the Lorentz force due to (i) electrostatic field \mathbf{E} created by atoms in the environment and/or by external charges, and (ii) external magnetic field \mathbf{B} :

$$\mathbf{F}_{\text{em}} = q(\mathbf{E} + \boldsymbol{\beta} \times \mathbf{B}). \quad (3)$$

The second term in (2), \mathbf{F}_{rd} , is a radiation damping force that accounts for the reaction of the emitted radiation on the motion of the charged particle, see, e.g. [20, 21]. Its action leads to a gradual decrease of the particle's energy. For ultra-relativistic projectiles of very high energies (tens of GeV and above) this force becomes quite noticeable, so that it must be accounted for to properly simulate the motion, see recent experiments [22–24]. The methodology that has been developed to incorporate \mathbf{F}_{rd} into the relativistic MD framework implemented in the MBN EXPLORER package is described in Ref.[25].

Applied to the passage of a charged particle through an atomic environment, the environment, the system (1) describes the classical motion of the particle in an electrostatic field of the atoms of the medium. In this case, the two terms on the right-hand side of eq. (3) depend on the intensity of the field, which can be calculated as is calculated as $\mathbf{E} = -\nabla\phi(\mathbf{r})$ where $\phi(\mathbf{r})$ is the potential of the field is equal to the sum of the potentials of the individual atoms.

$$\phi(\mathbf{r}) = \sum_j \phi_{\text{at}}(|\mathbf{r} - \mathbf{r}_j|), \quad (4)$$

where \mathbf{r}_j denotes the position vector of the nucleus of the j th atom. For a neutral atom, the potential $\phi(\mathbf{r})$ is a rapidly decreasing function at distances greater than the average atomic radius. Therefore, at each integration step of eq. (1), the sum in (4) can only include the atoms inside the sphere of a given cut-off radius ρ with the centre at \mathbf{r} . Typically ρ is chosen to be an order of magnitude larger than the average atomic radius. The search for such atoms is done using the linked cell algorithm implemented in the MBN EXPLORER package. As the particle passes through a medium, the environment is generated dynamically, so that the simulation box follows the moving particle. For a crystalline environment the positions of the atoms are generated taking into account random displacement from the nodes due to thermal vibrations. More detailed description on the algorithms used to compute the trajectories at various scales, including macroscopically large ones, are presented in Refs. [14, 15, 17, 19, 25].

The classical equations of motion (1) do not take into account for events of inelastic scattering of a projectile particle from individual atoms, which lead to the excitation or ionisation of the atom. These events result in two subsequent changes in the particle motion:

- A random decrease in the energy of the projectile (ionisation losses).

- A random change in the direction of the projectile motion characterised by two scattering angles, θ and ϕ , measured with respect to the instant velocity, \mathbf{v} .

Rigorous treatment of inelastic collision events can only be achieved by means of quantum mechanics. However, given the random, fast and local nature of such events, they can be incorporated into the classical mechanics framework according to their probabilities. This approach has been already implemented in MBN EXPLORER within the framework of irradiation-driven MD [26]. A similar methodology, described below, has been realised in the code to account for the ionising collisions. Its implementation followed the scheme presented in Ref. [27].

For an ultra-relativistic particle passing through a medium, the probability d^2W of the relative energy loss $d\Delta = d\varepsilon/\varepsilon$ over the path $ds \approx cdt$ due to ionising collision with quasi-free electrons can be calculated using the following expression (see, e.g., Eqs. (1.7)-(1.7b) in [28] and §33.2.7 in [29]):

$$\frac{d^2W}{d\Delta ds} = 2\pi r_0^2 q^2 \frac{n_e(\mathbf{r})}{\gamma \Delta^2}. \quad (5)$$

Here $r_0 = 2.818 \times 10^{-13}$ is the classical electron radius and $n_e(\mathbf{r})$ is the local volume density of electrons. In the points $\mathbf{r} \neq \mathbf{r}_j$, i.e. not at the nuclei, the density is related to the potential (4) via the Poisson equation:

$$n_e(\mathbf{r}) = \frac{1}{4\pi e} \nabla^2 \sum_j \phi_{\text{at}}(|\mathbf{r} - \mathbf{r}_j|). \quad (6)$$

In a single collision, the value of relative energy loss $\Delta = (\varepsilon - \varepsilon')/\varepsilon$, where ε and $\varepsilon' < \varepsilon$ are the particle's energies before and after the collision, lies within the interval

$$\Delta_{\min} \leq \Delta \leq \Delta_{\max}, \quad (7)$$

$$\Delta_{\min} = I/\varepsilon, \quad \Delta_{\max} \approx \begin{cases} \frac{2\gamma\xi}{1+2\gamma\xi} & \text{for a heavy particle} \\ 1 & \text{for a positron} \\ 0.5 & \text{for an electron} \end{cases} \quad (8)$$

where ξ is the electron-to-projectile mass ratio and I denotes the atomic ionization potential, which can be estimated as $I = 16Z^{0.9}$ eV within the Thomas-Fermi model (Z is the atomic number).

As written, the distribution (5) holds for $\Delta \ll 1$. However, since a probability of collisions with $\Delta \gtrsim 1$ is negligibly small, Eq. (5) can be applied to the whole range of the Δ values.

At each step Δt of integration of Eqs. (1) an ionising collision is treated as a probabilistic event. Once it occurs and the value Δ is determined, one calculates a round scattering angle θ measured with respect to the instant velocity $\mathbf{v}(t)$:

$$\cos \theta = \sqrt{\frac{\gamma+1}{\gamma-1}} \sqrt{\frac{1-\Delta-\gamma^{-1}}{1-\Delta+\gamma^{-1}}} - \frac{\Delta(\xi-1)}{\sqrt{\gamma^2-1}\sqrt{(1-\Delta)^2-\gamma^{-2}}} \quad (9)$$

The second scattering angle ϕ is not restricted by any kinematic relations, and its value is generated as a uniform random deviate between 0 and 2π .

The algorithm of random generation of the Δ and θ values is as follows [27].

The two-fold probability (5) is normalized as follows

$$\int_0^{L_{\text{ion}}} \int_{\Delta_{\text{min}}}^{\Delta_{\text{max}}} \frac{d^2W}{d\Delta ds} d\Delta ds = 1 \quad (10)$$

where L_{ion} is a spatial path over which the probability of an ionising collision with an arbitrary energy transfer is equal to one:

$$L_{\text{ion}}^{-1} = \frac{2\pi r_0^2 q^2 n_e(\mathbf{r})}{\gamma} \frac{1}{\Delta_0}, \quad \Delta_0 = \frac{\Delta_{\text{max}} \Delta_{\text{min}}}{\Delta_{\text{max}} - \Delta_{\text{min}}} \approx \Delta_{\text{min}}. \quad (11)$$

Therefore, the probability of an ionising collision with the energy transfer Δ to occur over the path $\Delta s = c\Delta t$ is given by

$$dW = \frac{\Delta s}{L_{\text{ion}}} P(\Delta) d\Delta, \quad P(\Delta) = \frac{\Delta_0}{\Delta^2} \quad (12)$$

where the factor $P(\Delta) d\Delta$ stands the normalized probability of the relative energy loss between Δ and $\Delta + d\Delta$.

To simulate the probability of an ionising collision to take place, a uniform random deviate $x \in [0, 1]$ is generated and compared with $\Delta s/L_{\text{ion}}$. If $x \leq \Delta s/L_{\text{ion}}$ then the collision happens and another random deviate Δ is generated and used in Eq. (9) to calculate θ .

The values of Δ , θ and ϕ obtained are used further to modify the velocity and energy of the projectile at the start of the next integration step.

To account for or to disregard the ionising collisions the following schemes are implemented in MBN EXPLORER:

- the local electron density $n_e(\mathbf{r})$ is calculated using Eq. (6) where atomic potentials ϕ_{at} are considered within the frameworks of the Molière [30] or Fernandes Pacios [31] approximations.

- the local density is substituted with the average electron density in the amorphous medium: $n_e(\mathbf{r}) = Zn_{\text{at}}$ where n_{at} stands for the volume density of atoms in the amorphous environment,
- to disregard the ionising collisions one sets $n_e(\mathbf{r}) \equiv 0$.

III. CASE STUDIES

The case studies presented below refer to the channeling of $\varepsilon = 270, 855$ and 1500 MeV electrons (e^-) and 530 MeV positrons (e^+) in single diamond (C), silicon (Si) and germanium (Ge) crystals oriented, with respect to the incident beam, along the (110) and (111) planar directions. The beams were assumed to be ideally collimated. The values of crystal thickness L along the beam used in the simulations are (i) $200, 200, 400$ microns for $270, 855, 1500$ MeV electrons, respectively, and (ii) 1000 microns for the positrons. For electrons, the aforementioned energy range corresponds that available at the Mainz Mikrotron (MAMI) facility [32]. A number of channeling experiments with the electron beam have been carried out at MAMI with various crystal targets during the last one and a half decade [6, 33–36]. More recently, within the framework of the TECHNO-CLS project [13], a new 530 MeV positron beam line has been designed at MAMI [37] and the first experimental tests with the positron beam have been carried out [38, 39].

A. Statistical analysis of the channeling process

For each case study approximately $N_0 = 1.2 \times 10^4$ of trajectories have been simulated and analyzed. Randomness in the "entry conditions" leads to diversity in the scattering events for the different projectiles at the crystal entrance. Consequently, not all particles start their propagation moving in the the channeling regime. To quantify this property, the acceptance \mathcal{A} can be introduced as the ratio of the number N_{acc} of particles accepted into the channeling regime to the total N_0 number of particles: $\mathcal{A} = N_{\text{acc}}/N_0$.

A significant methodological issue pertains to the formulation of a criterion for distinguishing between channeling and non-channeling regimes of projectiles' motion. Depending on the theoretical approach employed to describe the interaction of a projectile with a crystalline environment, the criterion can be introduced in various ways. For instance, within

the continuous potential framework, it is straightforward to define the channeling particles as those with transverse energies less than the height of the inter-planar (or inter-axial) potential barrier ΔU . Within this framework, the acceptance is determined at the entrance to the crystal and can be defined as the ratio of the number of particles with transverse energy less than ΔU to the total number of particles. Within the framework of relativistic MD, the simulations are based on resolution of the EM (1), incorporating the interaction of a projectile particle with individual atoms of the crystal, as would be observed in reality. The potential experienced by the projectile varies rapidly during its motion, thereby coupling the transverse and longitudinal degrees of freedom. It is therefore necessary to propose an alternative criterion for identifying the channeling segments in the projectile's trajectory. In the case of planar channeling, it can be postulated that a projectile is captured in the channeling mode when the sign of its transverse velocity undergoes a minimum of two changes within a single channel. [15].

The collisions (both elastic and inelastic ones) with the crystal atoms lead to a gradual decrease in the number of channeling particles, which were initially accepted, with the penetration distance. This dependence can be characterized by the fraction $f_{\text{ch},0}(z) = N_{\text{ch},0}(z)/N_{\text{acc}}$ [19]. Here $N_{\text{ch},0}(z)$ is the number of particles which have been accepted at the entrance ($z = 0$) and channeled to the distance z , where they dechannel.

The non-accepted particles, as well as the dechanneled particles, experience unrestricted over-barrier motion. However, due to the collisions, they can be captured in the channeling mode (rechanneled) at some point in the bulk. With the notation $N_{\text{ch}}(z)$ as the total number of channeling particles at distance z , one can consider the fraction $f_{\text{ch}}(z) = N_{\text{ch}}(z)/N_{\text{acc}}$, which accounts for the rechanneling process.

The fraction $f_{\text{ch},0}(z)$ can be used to quantify the dechanneling effect in terms of the *penetration length* L_{p} , which stands for the mean length of the channeling segment of the trajectory of an accepted particle:

$$L_{\text{p}} = \int_0^L f_{\text{ch},0}(z) dz. \quad (13)$$

As defined, L_{p} depends on the crystal length L . However, for sufficiently large values of L , for which $f_{\text{ch},0}(z) \rightarrow 0$ so that the contribution of the interval $[L, \infty]$ to the integral is negligibly small, Eq. (13) gives the value of L_{p} independent of L .

For both electrons and positrons, an analytical fit for $f_{\text{ch},0}(z)$ can be constructed using

parameters calculated within the diffusion theory of the dechanneling process (see, e.g., [2, 40, 41]). Apart from some initial segment $[0, z_0]$, this fraction can be approximated by an exponentially decaying function:

For both electrons and positrons, an analytical fit can be constructed for $f_{\text{ch},0}(z)$ using parameters calculated within the diffusion theory of the dechanneling process (see e.g., [2, 40, 41]). Apart from some initial segment $[0, z_0]$, this fraction can be approximated by an exponentially decaying function:

$$f_{\text{ch},0}(z) \approx \widetilde{f}_{\text{ch},0}(z) = e^{-\frac{z-z_0}{L_d}} \quad (14)$$

where z_0 and L_d are fitting parameters. It can be shown [19] that the quantities L, L_p, z_0 and \widetilde{L}_d are related as follows: $L_p = z_0 + L_d (1 - e^{-(L-z_0)/L_d})$. In the case of a thick crystal, $L \gg L_d$, one finds $L_p \approx z_0 + L_d$.

Unlike $f_{\text{ch},0}(z)$, the dependence of the fraction $f_{\text{ch}}(z)$ on the penetration distance is sensitive to the sign of the charge of the projectile. This will be discussed later in the paper.

Figures 1-3 and 4 show the dependence of the channeling fractions $f_{\text{ch},0}(z)$ (solid curves) and $f_{\text{ch}}(z)$ (dashed curves) for electrons and positrons, respectively. The error bars indicate the statistical uncertainties due to the finite number of the simulated trajectories. In each graph, the fractions calculated with account for ionising collisions (marked 'yes') are compared with those calculated without the ionising collisions.

Let us first discuss the electron channeling, Figs. 1-3. The main feature seen in all graphs is that within the statistical errors the 'yes' and 'no' dependencies are virtually the same. The results presented indicate that for electrons the ionising collisions can be disregarded in the quantitative description of the dechanneling and rechanneling processes. This can be understood recalling that negatively charged particles experience channeling motion in the vicinity of the atomic planes. Therefore, they experience rather close collisions (i.e. with comparatively small impact parameter) with the crystal atoms. For these impact parameters, the change in the transverse momentum of the particle is mainly due to elastic scattering from the static atomic potential rather than inelastic scattering from the atomic electrons. The decrease in transverse momentum can cause the particle to be re-channeled and thus contribute to the channeling fraction $f_{\text{ch}}(z)$.

As the penetration distance increases, the function $f_{\text{ch}}(z)$ decreases much more slowly than the fraction $f_{\text{ch},0}(z)$. In Ref. [19] it was shown that $f_{\text{ch}}(z)$ can be well approximated

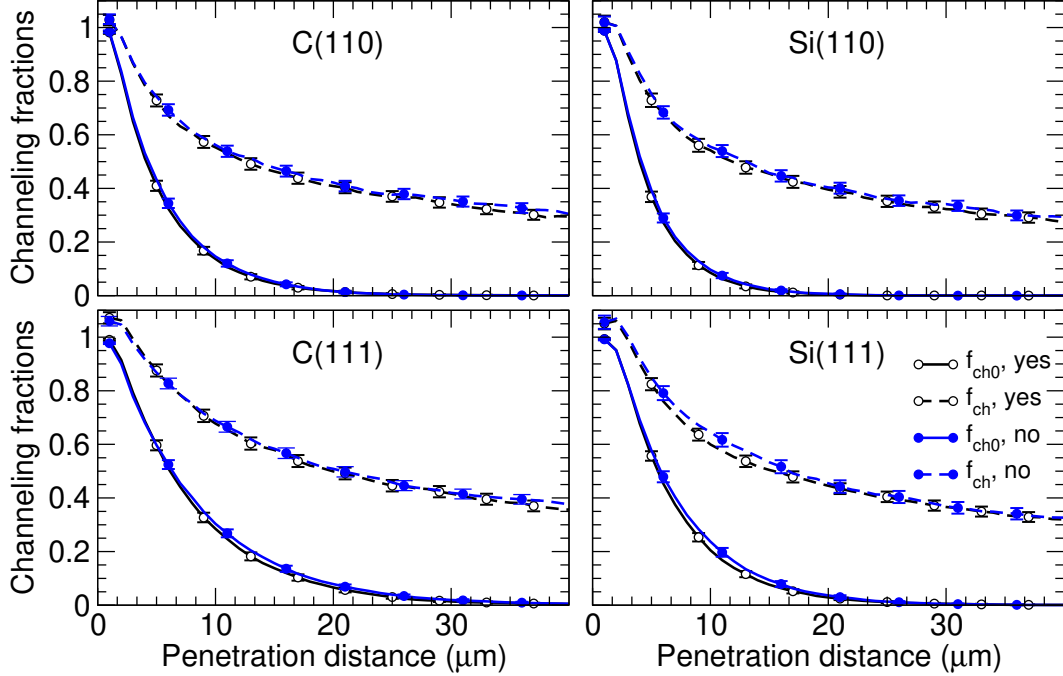


FIG. 1. Channeling fractions $f_{ch,0}$ (solid lines) and f_{ch} (dashed lines) versus penetration distance z for 270 MeV electrons in diamond (left column) and silicon (right column) crystals. The upper row corresponds to the planar channeling along the (110) direction, the lower row - to the (111) direction. Curves with open circles show the results obtained taking into account the ionising collisions (labelled 'yes' in the common legend placed in the upper right graph). Curves with filled circles represent the dependencies calculated without ionising collisions (labelled 'no' in the legend). The simulations were performed for the beams of zero divergence.

by the following fitting formula:

$$\widetilde{f}_{ch}(z) \approx \text{erf} \left(\beta \sqrt{\frac{\varepsilon}{z}} \right) \quad (15)$$

where $\text{erf}(\cdot)$ stands for the error function and β is the fitting parameter. It is mentioned in the cited paper that if ε is measured in MeV and z in microns then as an initial guess for β one can use the value of $(L_{\text{rad}}U_0)^{1/2}/106$ where L_{rad} is the radiation length (in cm) and U_0 is the depth of the interplanar potential (in eV) [19]. For sufficiently large distances $\text{erf} \left(\beta \sqrt{\varepsilon/z} \right) \propto z^{-1/2}$.

To illustrate the applicability of (15) we present Fig. 5 (left graph), which compares dependencies $f_{ch}(z)$ obtained from the simulations with the fitting function $\widetilde{f}_{ch}(z)$.

Table I summarises the values of the aforementioned parameters namely the acceptance

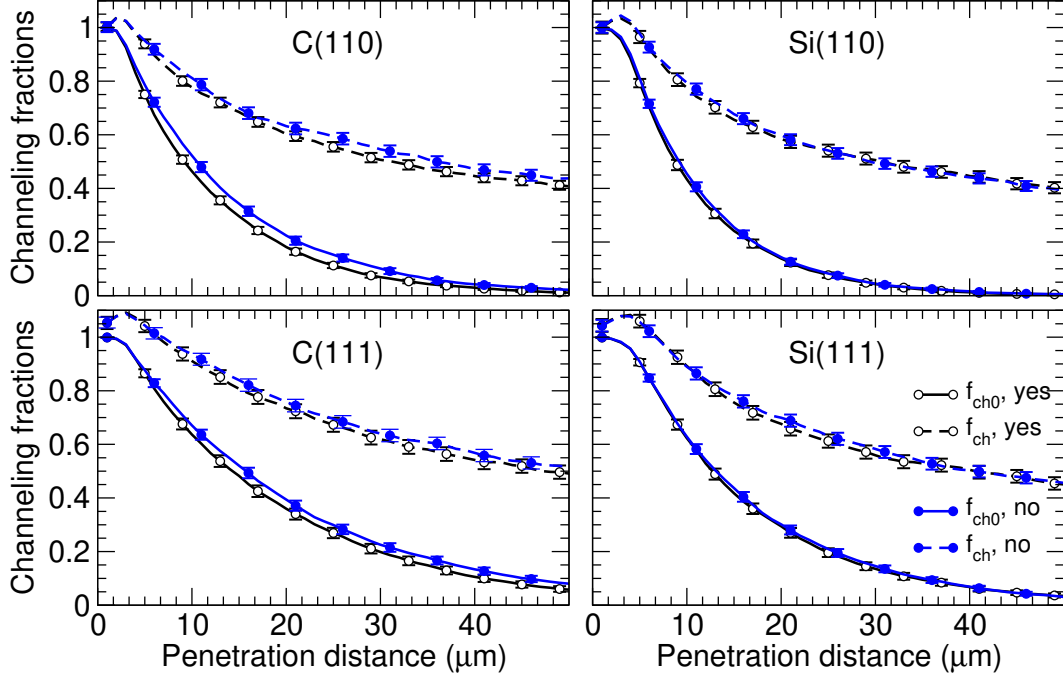


FIG. 2. Same as in Fig. 1 but for 855 MeV electrons.

\mathcal{A} , the penetration distance L_p , the asymptotic dechanneling length L_d and the fitting parameter β calculated for $\varepsilon = 270, 855$ and 1500 MeV electrons in different planar channels. For each channel shown, the results obtained with and without taking the ionising collisions into account are shown in the first and second rows, respectively.

The results of the analysis of the channeling phenomenon for 530 MeV positrons are presented in Figs. 4 and 5 (right graph), and Table II. In the figures, the curves shown for the (111) orientation of the crystals refer to the "wide" part of the (111) channel, which exhibits much higher channeling efficiency than the "narrow" part (see illustrative data in Appendix A).

As demonstrated in Fig. 4, the dependencies $f_{ch,0}(z)$ and $f_{ch}(z)$ exhibit two features that diverge distinctly from the electron channeling case.

Firstly, it is evident that accounting for the ionising collisions results in a much steeper decrease of the fractions with the penetration distance. This is not surprising since positrons effectively channel in the spatial regions between atomic planes. Therefore, statistically, they experience much more distant collisions with atoms than channeling electrons. At large impact parameters, the inelastic channels dominate in the total cross section of the collision between an ultra-relativistic projectile and an atom. Consequently, the increase in

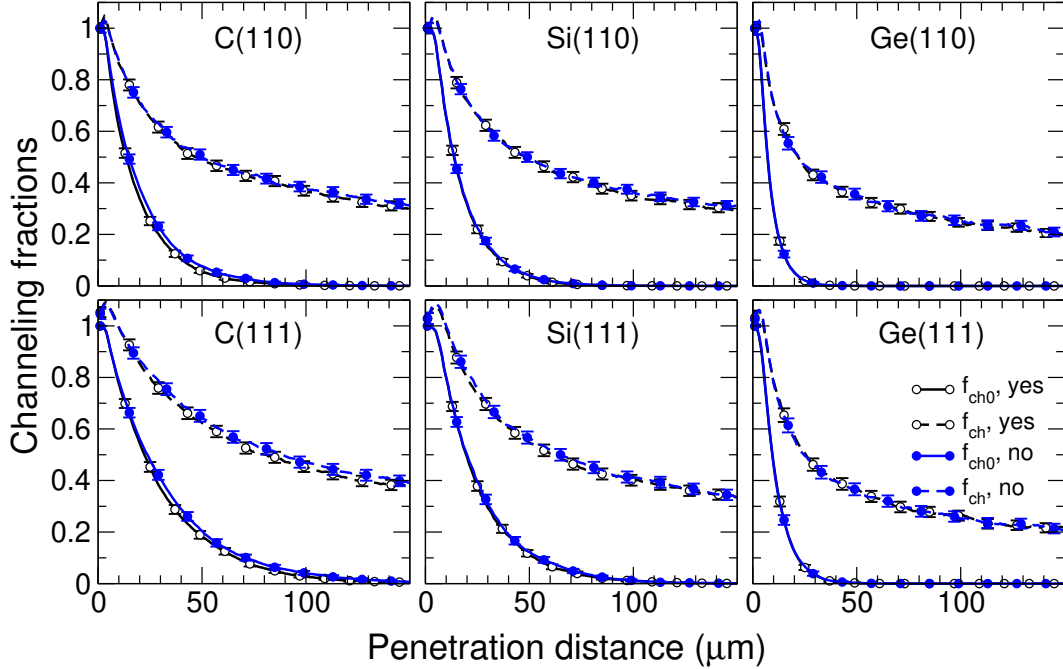


FIG. 3. Same as in Fig. 1 but (i) for 1500 MeV electrons, and (ii) adding the case of channeling in the (110) and (111) channels in germanium crystal, left column.

the transverse momentum occurs at a higher rate, leading to a faster decrease of the fractions. It should be mentioned, nevertheless, that dechanneling due to the elastic collisions is not at all negligible. A comparison of the dependencies, calculated with and without ionisation losses, demonstrates that the elastic scattering provides from 30 % (in the case of diamond) up to 50 % (for Si(111) and Ge(110)) of the total decrease in the channeling fractions $f_{ch,0}(z)$ and $f_{ch}(z)$ at the crystal exit.

The second feature to be mentioned is that the replenishment of the channeling fraction due to the rechanneling phenomenon is much less efficient than in the case of electron channeling. Consequently, the dependencies $f_{ch}(z)$ decrease much faster. In the range of penetration distances $z \leq 1000 \mu\text{m}$, considered in the simulations, the behaviour of these dependencies can be approximated as an exponentially decaying function $\propto \exp(-z/L_r)$, i.e. the same as for $f_{ch,0}(z)$, Eq. (14), but with different fitting parameter L_r . Figure 5*right* compares the dependencies $f_{ch}(z)$ obtained from the simulations with the fitting function. The values of L_r are shown in Table II together with the acceptance \mathcal{A} and the asymptotic dechanneling length L_d .

TABLE I. Acceptance \mathcal{A} , dechanneling length L_d (Eq. (14)), penetration length L_p (Eq. (13)) and fitting parameter β (Eq. (15)) calculated for 270, 855 and 1500 MeV electrons incident on the oriented crystals. Values of L_p and L_d are in microns, β is in $(\mu\text{m}/\text{MeV})^{1/2}$. For each channel, the results obtained with and without taking the ionising collisions into account are shown in the first and second rows, respectively. All data refer to the electron beams of zero divergence.

	$\varepsilon = 270 \text{ MeV}$				$\varepsilon = 855 \text{ MeV}$				$\varepsilon = 1.5 \text{ GeV}$			
	\mathcal{A}	L_d	L_p	β	\mathcal{A}	L_d	L_p	β	\mathcal{A}	L_d	L_p	β
C(110)	0.73	4.4 ± 0.2	5.5 ± 0.3	0.104 ± 0.006	0.74	10.5 ± 0.4	12.5 ± 0.5	0.092 ± 0.005	0.74	16.3 ± 0.7	18.9 ± 0.9	0.087 ± 0.004
	0.74	4.5 ± 0.1	5.7 ± 0.3		0.76	12.0 ± 0.6	14.2 ± 0.7		0.76	17.6 ± 0.7	20.8 ± 1.0	
C(111)	0.68	7.0 ± 0.3	8.2 ± 0.4	0.125 ± 0.005	0.70	17.0 ± 0.8	19.3 ± 1.0	0.111 ± 0.004	0.71	27.4 ± 1.2	30.5 ± 1.5	0.110 ± 0.004
	0.69	7.3 ± 0.2	8.6 ± 0.4		0.71	18.6 ± 0.8	21.2 ± 1.1		0.72	29.0 ± 1.2	32.7 ± 1.7	
Si(110)	0.64	3.5 ± 0.2	5.0 ± 0.2	0.097 ± 0.005	0.66	8.5 ± 0.4	11.4 ± 0.5	0.090 ± 0.004	0.74	13.8 ± 0.6	17.9 ± 0.8	0.085 ± 0.003
	0.64	3.7 ± 0.2	5.2 ± 0.2		0.67	8.7 ± 0.4	11.8 ± 0.5		0.76	14.1 ± 0.5	18.2 ± 0.7	
Si(111)	0.62	5.1 ± 0.2	7.1 ± 0.3	0.111 ± 0.006	0.65	13.2 ± 0.6	16.9 ± 0.8	0.102 ± 0.004	0.66	20.3 ± 1.0	25.7 ± 1.2	0.096 ± 0.004
	0.62	5.5 ± 0.3	7.4 ± 0.3		0.65	13.6 ± 0.6	17.3 ± 0.8		0.67	21.1 ± 1.2	26.5 ± 1.3	
Ge(110)									0.59	5.7 ± 0.4	8.7 ± 0.3	0.057 ± 0.003
									0.59	5.8 ± 0.2	8.8 ± 0.4	
Ge(111)									0.57	7.9 ± 0.8	11.5 ± 0.5	0.061 ± 0.003
									0.58	8.0 ± 0.8	11.6 ± 0.5	

TABLE II. Acceptance \mathcal{A} , dechanneling length L_d and the parameter L_r (both in microns) calculated 530 MeV positrons with taking the ionising collisions into account. For the (111) orientation, the \mathcal{A} and L_d values indicated in the upper row pertain to the "wide" part of the channel, while the lower row corresponds to the "narrow" part. The values of L_r refer to the "wide" part only. The data refer to the positron beam of zero divergence.

	C(110)	C(111)	Si(110)	Si(111)	Ge(110)	Ge(111)
\mathcal{A}	0.94	0.78	0.93	0.75	0.92	0.74
		0.17		0.18		0.17
L_d	305 ± 15	445 ± 15	640 ± 15	1060 ± 30	520 ± 10	900 ± 25
		30 ± 3		44 ± 4		27 ± 2
L_r	470 ± 10	620 ± 15	800 ± 20	1230 ± 25	615 ± 15	990 ± 20

B. Spectral distribution of emitted radiation

In this Section, we present several case studies of the photon emission spectra by 855 and 1500 MeV electrons and 530 MeV positrons. A more extensive presentation and detailed analysis will be published elsewhere.

For each simulated trajectory, the spectral-angular distribution $d^3E/d(\hbar\omega)d\Omega$ of the radiation of energy $\hbar\omega$ emitted within the solid angle $d\Omega \approx \theta d\theta d\phi$ (where θ and ϕ are the polar angles of the emission direction) is calculated numerically following the algorithm outlined in Ref. [15]. The spectral distribution of energy radiated within the cone $\theta_0 \ll 1$ along the incident beam and averaged over all trajectories is calculated using the following formula:

$$\frac{dE(\theta \leq \theta_0)}{d(\hbar\omega)} = \frac{1}{N_0} \sum_{n=1}^{N_0} \int_0^{2\pi} d\phi \int_0^{\theta_0} \theta d\theta \frac{d^3E_n}{d(\hbar\omega) d\Omega}. \quad (16)$$

The sum is carried out over all simulated trajectories of the total number N_0 ; as a result it takes into account the radiation emitted from the channeling segments of the trajectories as well as from those corresponding to the non-channeling regime.

The spectral distributions of radiation emitted by electrons are presented in Fig. 6. The upper row corresponds to 855 MeV electrons propagating through crystalline targets with a thickness of 200 μm , while the distributions for 1500 MeV electrons in 400 μm thick crystals

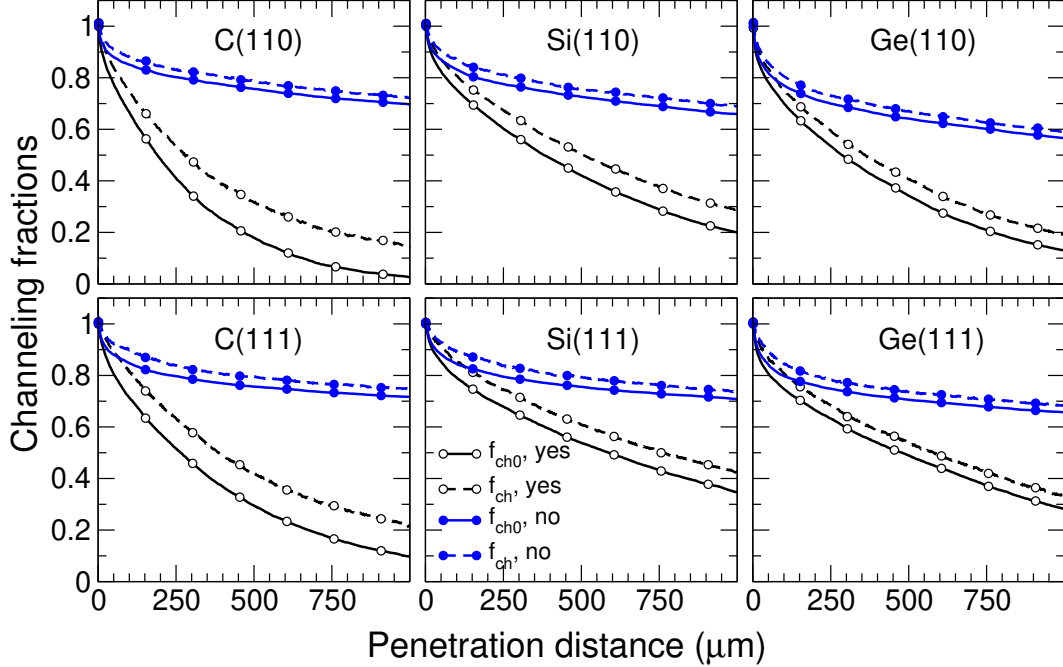


FIG. 4. Same as in Fig. 3 but for 530 MeV positrons. This paper presents a quantitative analysis of the impact of inelastic collisions of ultra-relativistic electrons and positrons, passing through oriented crystalline targets, on the channeling efficiency and on the intensity of the channeling radiation. The analysis is based on the numerical simulations of the channeling process performed using the MBN EXPLORER software package. The ionising collisions, being random, fast and local events, are incorporated into the classical molecular dynamics framework according to their probabilities. This methodology is outlined in the paper. The case studies presented refer to electrons with energy ε ranging from 270 to 1500 MeV and positrons with $\varepsilon = 530$ MeV incident on thick (up to 1 mm) single diamond, silicon and germanium crystals oriented along the (110) and (111) planar directions. In order to elucidate the role of the ionising collisions, the simulations were performed with and without account for the ionising collisions. The case studies presented demonstrate that both approaches yield highly similar results for the electrons. For the positrons, the ionising collisions reduce significantly the channeling efficiency. However, it has been observed that this effect does not result in a corresponding change in the radiation intensity. The dependencies for the (111) orientations are related to the "wide" part of the channel.

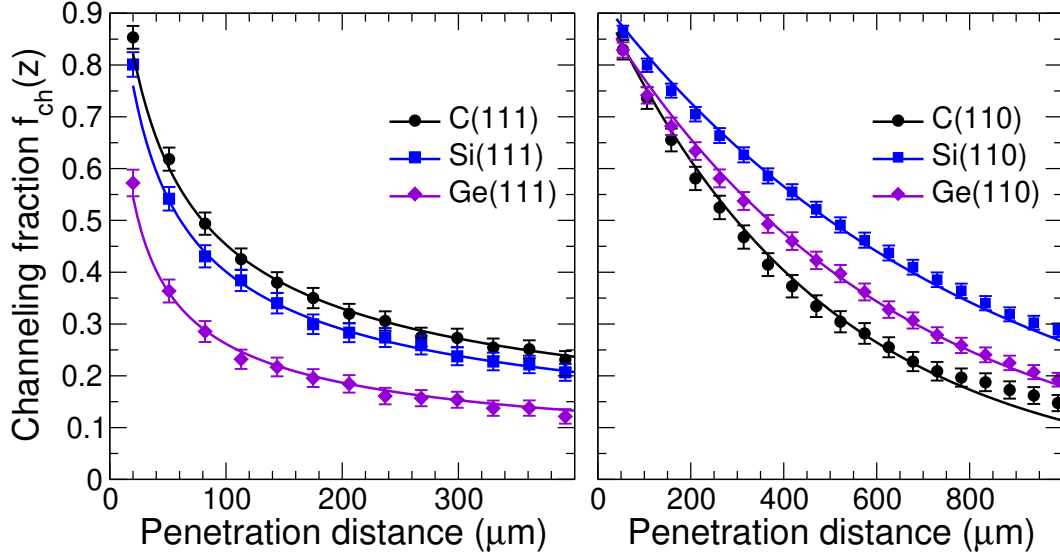


FIG. 5. Channeling fraction $f_{ch}(z)$ for 1500 MeV electrons (left) and 530 MeV positrons (right). The crystal orientation is indicated in the legends. The symbols show the results of the simulations with ionising collisions taken into account. The solid curves represent the fitting data calculated using Eq. (15) for electrons and the approximation $\widetilde{f}_{ch}(z) \propto \exp(-z/L_r)$ for positrons. The values of the fitting parameters β and L_r are given in Tables I and II, respectively.

are shown in the graphs in the lower row. For the lower energy, the spectra were computed for the cone with $\theta_0 = 3$ mrad, which exceeds the natural emission cone $1/\gamma$ by a factor of approximately five. For the higher energy, the cone considered 3 mrad is approximately $3/\gamma$. The common legend placed in the top-right graph indicates the crystals' orientation as well as marks the distributions calculated with account for ionising collisions ('yes') and without the ionising collisions ('no'). For the sake of comparison, the dashed-dotted line in each graph shows the spectrum of bremsstrahlung emitted in the amorphous medium of the same thickness. These spectra were calculated within the Bethe–Heitler approximation [42, 43].

For both energies of the electron beam the distributions are calculated in the photon energy ranges where the spectrum is dominated by the channeling radiation [44]. For the purpose of this paper it is important to note that, similar to the channeling fractions, the account for the ionising collision does not affect the spectral distributions. The most significant discrepancy (of approximately 10 per cent in the maximum of the spectra) between the 'yes' and 'no' curves is observed for 855 MeV electrons in the diamond targets.

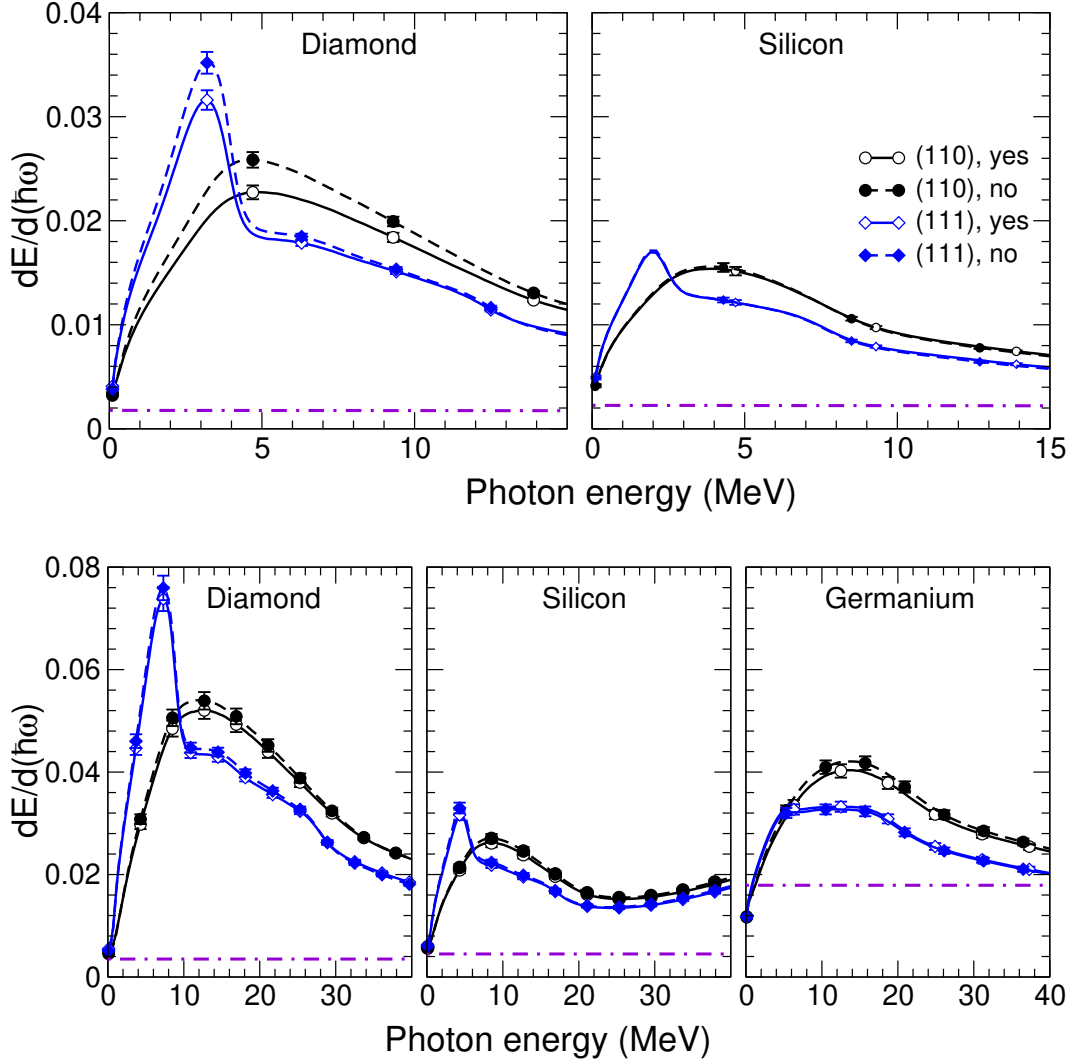


FIG. 6. Spectral distribution of the radiation emitted by 855 MeV (upper row) and 1500 MeV (lower row) electrons channeled in (110) and (111) channels in the diamond, silicon and germanium crystals, as indicated. The solid curves show the results obtained taking into account the ionising collisions (labelled 'yes' in the common legends placed in the upper right graph). The dashed curves represent the dependencies calculated without ionising collisions (labelled 'no' in the legend). The spectra shown correspond to the crystal thicknesses $L = 200$ and $400 \mu\text{m}$ and the emission cones $\theta_0 = 3$ and 1 mrad for the 855 and 1500 MeV projectiles, respectively. The dashed-dotted lines show the spectrum of the incoherent bremsstrahlung emitted in the amorphous target of the same thickness.

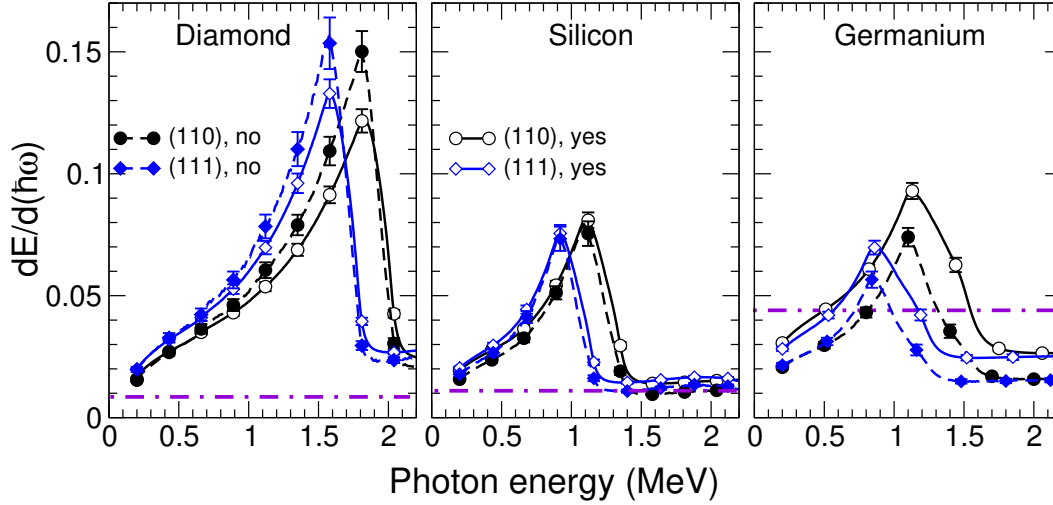


FIG. 7. Same as in Fig. 6 but for 530 MeV positrons. In all cases the crystal thicknesses is $L = 1000 \mu\text{m}$ and the emission cone $\theta_0 = 1 \text{ mrad}$. The dashed-dotted lines show the spectrum of the incoherent bremsstrahlung calculated in the Bethe-Heitler approximation.

The results for the spectral distributions of radiation by 530 MeV positrons in $L = 1000 \mu\text{m}$ -thick diamond, silicon and germanium oriented crystals are presented in Fig. 7. In all cases the emission cone is $\theta_0 = 1 \text{ mrad} \approx 3/\gamma$.

Considering a significant decline in channeling efficiency due to ionising collisions, see Fig. 4, one could expect to have a similar impact on the spectral distribution of the channeling radiation. It is seen that when ionising collisions are taken into account (the solid curves marked 'yes' in the legend), the peak value of the channeling radiation decreases by approximately 20-25 per cent for diamond and germanium, and remains virtually unchanged for silicon crystal. A possible explanation for this feature is based on the assumption that, although ionising collisions lead to a reduction in the average length of the channeling segments they also lead to a gradual increase in the amplitude of the channeling oscillations for the channeling particle. The former phenomenon tends to reduce the intensity of the channeling radiation, while the latter has the opposite effect. A more detailed quantitative analysis of this assumption is currently on the way.

IV. CONCLUSIONS

A quantitative analysis of the impact of inelastic collisions on the channeling efficiency and the radiation emission by 270-1500 MeV electrons and 530 MeV positrons incident on diamond, silicon and germanium single crystals oriented along the (110) and (111) planar directions has been reported. The crystals thickness along the incident beam was 200-400 μm for the electrons and 1000 μm for the positrons.

The simulations were performed by means of the MBN EXPLORER software package within the framework of classical relativistic MD. The incorporation of inelastic scattering events of projectile particles from crystal atoms into the classical framework was conducted according to their probabilities.

In order to elucidate the role of the ionising collisions, calculations were performed of the channeling fractions versus the penetration distance and of the spectral distribution of the emitted radiation, with and without account for these collisions.

The case studies presented for the electron beams have demonstrated that both approaches lead to very close results. The largest impact of ionising collisions on the values of the channeling fractions and of the channeling radiation intensity, seen for the diamond targets, is on the level of ten per cent. This discrepancy is significantly reduced in the heavier crystals. A comparatively weak role for ionising collisions can be explained by recalling that electrons channel in the vicinity of atomic planes. In this regime, the change in the transverse energy of the particle is mainly due to elastic scattering from the static atomic potential rather than inelastic scattering from atomic electrons.

The situation is less straightforward for positrons. They channel into the spatial regions between the atomic levels and therefore experience more distant collisions in which the inelastic channels dominate in the total cross section of a scattering from an atom. The simulations of the channeling motion have supported this conclusion leading to a much faster decrease in the channeling fractions with increasing penetration distance. The dechanneling rate due to inelastic collisions increases, ranging from 50 per cent (for Si(111) and Ge(110)) up to 70 per cent (for diamond) of the total dechanneling rate. However, the increase in the dechanneling rate does not lead to a comparable change in the radiation emission spectra. This phenomenon may be explained by the assumption that ionising collisions reduce the average length of the channeling segments, but increase the amplitude of the channeling

oscillations. The former reduces the intensity of the channeling radiation, while the latter increases it. A more detailed quantitative analysis of the particle dynamics and a more comprehensive presentation of the data on the radiation emission spectra will be presented elsewhere.

ACKNOWLEDGEMENTS

We acknowledge support by the European Commission through the N-LIGHT Project within the H2020-MSCA-RISE-2019 call (GA 872196) and the EIC Pathfinder Project TECHNO-CLS (Project No. 101046458). We also acknowledge the Frankfurt Center for Scientific Computing (CSC) for providing computer facilities.

Appendix A: The (111) interplanar potentials in diamond, silicon and germanium crystals

The results presented in the main text have been obtained using the all-atom relativistic MD approach implemented in the MBN EXPLORER software package [14, 15, 17]. This approach goes beyond the continuous potential model [1]. Therefore, the numerical data presented below in this section are for illustrative purposes only.

In crystals of the diamond group (diamond itself, silicon, germanium) the (111) crystallographic planes are arranged with two different alternating spacings. Expressed in terms of the lattice constant a , the wide interplanar distance is $d_W = 0.75a/\sqrt{3}$ and the narrow spacing is three times less, $d_N = 0.25a/\sqrt{3}$. The channeling motion of a positively charged projectile particle occurs in between two neighbouring planes. Consequently, in the crystal with the (111) orientation there are wide and narrow positron channels.

Figure 8 illustrates the continuous interplanar potentials in the wide and narrow (111) positron channels in the diamond, silicon and germanium crystals. The vertical dashed lines mark the positions of the crystallographic (111) planes. In each case, the interplanar potential is calculated by summing the continuous potentials U of individual planes. In turn, the potentials U are calculated by averaging out the potentials of individual atoms, considering their displacement from the nodal positions due to the thermal vibrations. The dependencies presented refer to a temperature $T = 300$ °C. The solid and dashed curves

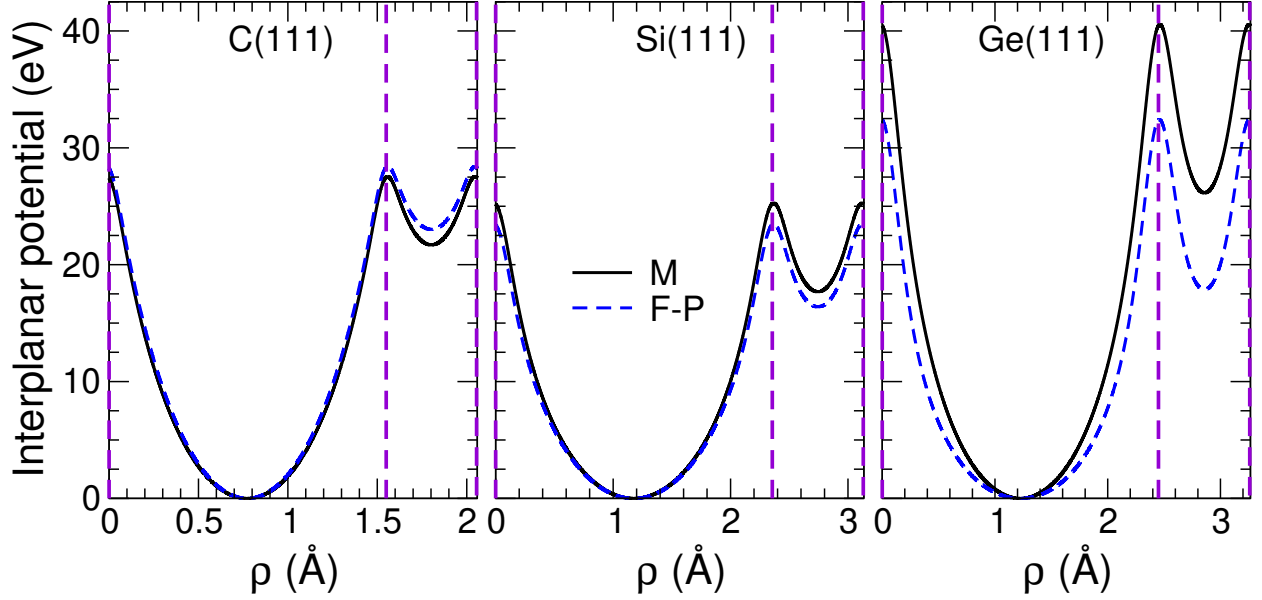


FIG. 8. Continuous interplanar potential for a positron in the diamond (C), silicon and germanium crystals with the (111) orientation. The vertical dashed lines mark the positions of the crystallographic (111) planes and illustrate the wide and narrow channels. The solid and dashed curves represent the potentials calculated using the Molière (M) [30] and Fernandes Pacios (F-P) [31] parametrisations of the atomic potentials, respectively.

in the figure represent the potentials calculated using the Molière (M) [30] and Fernandes Pacios (F-P) [31] parametrisations of the atomic potentials, respectively. More technical details on the calculation of the continuous planar potentials can be found in Ref. [19].

It is clear that, in all cases, the potential well in the wide channel is much deeper. This, and the big difference in the widths of the channels, indicates that the positron channeling efficiency of the wide channels is much higher than that of the narrow channels. This is also shown by the numerical simulations, which show that the dechanneling length, L_d in narrow channels is one order of magnitude less than in wide channels (see Table II).

REFERENCES

-
- [1] J. Lindhard, Influence of crystal lattice on motion of energetic charged particles, K. Dan. Vidensk. Selsk. Mat. Fys. Medd. **34**, 1 (1965).
- [2] V. M. Biryukov, Y. A. Chesnokov, and V. I. Kotov, *Crystal Channeling and its Application at High-Energy Accelerators* (Springer Science & Business Media, Berlin/Heidelberg, Germany, 2013).
- [3] U. I. Uggerhøj, The interaction of relativistic particles with strong crystalline fields, Rev. Mod. Phys. **77**, 1131 (2005).
- [4] A. V. Korol, A. V. Solov'yov, and W. Greiner, *Channeling and Radiation in Periodically Bent Crystals (2nd ed.)* (Springer Series on Atomic, Optical, and Plasma Physics, vol. 69. Springer-Verlag, Heidelberg, New York, Dordrecht, London, 2014) p. 284.
- [5] A. V. Korol and A. V. Solov'yov, *Novel Light Sources beyond Free Electron Lasers* (Springer Nature Switzerland AG, 2022).
- [6] A. Mazzolari, E. Bagli, L. Bandiera, V. Guidi, H. Backe, W. Lauth, V. Tikhomirov, A. Berra, D. Lietti, M. Prest, E. Vallazza, and D. D. Salvador, Steering of a sub-GeV electron beam through planar channeling enhanced by rechanneling, Phys. Rev. Lett. **112**, 135503 (2014).
- [7] A. Mazzolari, M. Romagnoni, R. Camattari, E. Bagli, L. Bandiera, G. Germogli, V. Guidi, and G. Cavoto, Bent crystals for efficient beam steering of multi TeV-particle beams, Eur. Phys. J. C **78**, 720 (2018).
- [8] U. Wienands, T. W. Markiewicz, J. Nelson, R. J. Noble, J. L. Turner, U. I. Uggerhøj, T. N. Wistisen, E. Bagli, L. Bandiera, G. Germogli, V. Guidi, A. Mazzolari, R. Holtzapple, and M. Miller, Observation of deflection of a beam of multi-GeV electrons by a thin crystal, Phys. Rev. Lett. **114**, 074801 (2015).
- [9] W. Scandale, G. Arduini, R. Assmann, C. Bracco, S. Gilardoni, V. Ippolito, E. Laface, R. Losito, A. Masi, E. Metral, V. Previtalli, S. Redaelli, M. Silari, L. Tlustos, E. Bagli, S. Baricordi, P. Dalpiaz, V. Guidi, A. Mazzolari, D. Vincenzi, G. D. Mea, A. Lombardi, D. D. Salvador, E. Vallazza, D. Bolognini, S. Hasan, D. Lietti, V. Mascagna, A. Mattera, M. Prest, G. Cavoto, L. Ludovici, D. Mirarchi, R. Santacesaria, P. Valente, F. Murtas, A. Afonin, Y. Chesnokov,

- V. Maishev, I. Yazynin, A. Kovalenko, A. Taratin, A. Denisov, Y. Gavrikov, Y. Ivanov, L. Lapina, L. Malyarenko, V. Skorobogatov, V. Suvorov, S. Vavilov, N. Mokhov, D. Still, G. Robert-Demolaize, T. Markiewicz, and M. Oriunno, First results on the SPS beam collimation with bent crystals, *Phys. Lett.* **692B**, 78 (2010).
- [10] W. Scandale, G. Arduini, F. Cerutti, M. Garattini, S. Gilardoni, *et al.*, Focusing of 180 GeV/c pions from a point-like source into a parallel beam by a bent silicon crystal, *Nucl. Instrum. Method B* **446**, 15 (2019).
- [11] G. B. Sushko, A. V. Korol, and A. V. Solov'yov, Extremely brilliant crystal-based light sources, *Europ. Phys. J. D* **76**, 166 (2022).
- [12] A. V. Korol and A. V. Solov'yov, Atomistic modeling and characterization of light sources based on small-amplitude short-period periodically bent crystals, *Nucl. Instrum. Meth. B* **537**, 1 (2023).
- [13] <http://www.mbnresearch.com/TECHNO-CLS/Main>.
- [14] I. A. Solov'yov, A. V. Yakubovich, P. V. Nikolaev, I. Volkovets, and A. V. Solov'yov, MesoBioNano Explorer – A universal program for multiscale computer simulations of complex molecular structure and dynamics, *J. Comput. Phys.* **33**, 2412 (2012).
- [15] G. B. Sushko, V. G. Bezchastnov, I. A. Solov'yov, A. V. Korol, W. Greiner, and A. V. Solov'yov, Simulation of ultra-relativistic electrons and positrons channeling in crystals with MBN Explorer, *J. Comput. Phys.* **252**, 404 (2013).
- [16] G. Sushko, I. Solov'yov, and A. Solov'yov, Modeling MesoBioNano systems with MBN Studio made easy, *J. Mol. Graph. Model.* **88**, 247 (2019).
- [17] I. A. Solov'yov, A. V., Korol, and A. V. Solov'yov, *Multiscale Modeling of Complex Molecular Structure and Dynamics with MBN Explorer* (Springer International Publishing, Cham, Switzerland, 2017).
- [18] I. A. Solov'yov, A. V. Verkhovtsev, A. V. Korol, and A. V. Solov'yov, eds., *Dynamics of Systems on the Nanoscale* (Springer Nature Switzerland, Cham, Switzerland, 2022).
- [19] A. V. Korol, G. B. Sushko, and A. V. Solov'yov, All-atom relativistic molecular dynamics simulations of channeling and radiation processes in oriented crystals, *Europ. Phys. J. D* **75**, 107 (2021).
- [20] L. D. Landau and E. M. Lifshitz, *Course of Theoretical Physics, vol.2. The Classical Theory*

- of Fields* (London Pergamon, 1971).
- [21] J. D. Jackson, *Classical Electrodynamics, 3rd Edition* (John Wiley & Sons, Inc., 1999).
 - [22] T. N. Wistisen, A. Di Piazza, H. V. Knudsen, and U. I. Uggerhøj, Experimental evidence of quantum radiation reaction in aligned crystals, *Nature Communications* **9**, 1 (2018).
 - [23] T. N. Wistisen, A. Di Piazza, C. F. Nielsen, A. H. Justesen, Sørensen, and U. I. Uggerhøj, Quantum radiation reaction in aligned crystals beyond the local constant field approximation, *Phys. Rev. Res.* **1**, 033014 (2019).
 - [24] C. F. Nielsen, J. B. Justesen, A. H. Sørensen, U. I. Uggerhøj, and R. Holtzapple, Radiation reaction near the classical limit in aligned crystals, *Phys. Rev. D* **102**, 052004 (2020).
 - [25] G. B. Sushko, A. V. Korol, and A. V. Solov'yov, Atomistic modeling of the channeling process with radiation reaction force included, *Nucl. Instrum. Meth. B* **535**, 117 (2023).
 - [26] G. B. Sushko, I. A. Solov'yov, and A. V. Solov'yov, Molecular dynamics for irradiation driven chemistry: Application to the FEBID process, *Eur. Phys. J. D* **70**, 217 (2016).
 - [27] A. V. Korol, A. V. Solov'yov, and W. Greiner, The influence of the dechannelling process on the photon emission by an ultra-relativistic positron channelling in a periodically bent crystal, *J. Phys. G: Nucl. Part. Phys.* **27**, 95 (2001).
 - [28] B. Rossi and K. Greisen, Cosmic-ray theory, *Rev. Mod. Phys.* **13**, 240 (1941).
 - [29] M. Tanabashi and others (Particle Data Group), Review of particle physics, *Phys. Rev. D* **98**, 030001 (2018).
 - [30] G. Molière, Theorie der Streuung schneller geladener Teilchen I: Einzelstreuung am abgeschirmten Coulomb-Feld, *Z. f. Naturforsch. A* **2**, 133 (1947).
 - [31] L. F. Pacios, Simple analytical representation of atomic electron charge densities, electrostatic potentials, and local exchange potentials, *J. Comp. Chem.* **96**, 7294 (1992).
 - [32] <https://www.blogs.uni-mainz.de/fb08-nuclear-physics/accelerators-mami-mesa/the-mainz-microtron/>
 - [33] H. Backe, P. Kunz, W. Lauth, and A. Rueda, Planar channeling experiments with electrons at the 855 MeV Mainz Microtron MAMI, *Nucl. Instrum. Meth. B* **266**, 3835 (2015).
 - [34] H. Backe and W. Lauth, Channeling experiments with sub-GeV electrons in flat silicon single crystals, *Nucl. Instrum. Meth. B* **355**, 24 (2015).
 - [35] L. Bandiera, E. Bagli, G. Germogli, V. Guidi, A. Mazzolari, H. Backe, W. Lauth, A. Berra, D. Lietti, M. Prest, D. D. Salvador, E. Vallazza, and V. Tikhomirov, Investigation of the electromagnetic radiation emitted by sub-GeV electrons in a bent crystal,

- Phys. Rev. Lett. **115**, 025504 (2015).
- [36] H. Backe, D. Krambrich, W. Lauth, K. K. Andersen, J. L. Hansen, and U. I. Uggerhøj, Channeling and radiation of electrons in silicon single crystals and $\text{Si}_{1-x}\text{Ge}_x$ crystalline undulators, J. Phys. Conf. Ser. **438**, 012017 (2013).
- [37] H. Backe, W. Lauth, P. Drexler, P. Heil, P. Klag, B. Ledroit, and F. Stieleret, Design study for a 500 MeV positron beam at the mainz microtron mami, Europ. Phys. J. D **76**, 150 (2022).
- [38] A. Mazzolari, H. Backe, L. Bandiera, N. Canale, D. D. Salvador, P. Drexler, V. Guidi, P. Klag, W. Lauth, L. Malagutti, R. Negrello, G. Paterno, M. Romagnoni, F. Sgarbossa, A. Sytov, V. Tikhomirov, and D. Valzani, Observation of fine structure in channeling of particles in bent crystals, arXiv:2404.08459 (2024).
- [39] H. Backe, On planar (110) channeling of 500 MeV positrons and electrons in silicon semiconductor detectors, Nucl. Instrum. Meth. A **1059**, 168998 (2024).
- [40] T. Waho, Planar channeling of protons in Si and Ge, Phys. Rev. B **14**, 4830 (1976).
- [41] H. Backe, De-channeling in terms of instantaneous transition rates: computer simulations for 855 MeV electrons at (110) planes of diamond, Europ. Phys. J. D **76**, 153 (2022).
- [42] H. Bethe and W. Heitler, On the stopping of fast particles and on the creation of positive electrons, Proc. Roy. Soc. London. Series A **146**, 83 (1934).
- [43] H. A. Bethe and L. C. Maximon, Theory of bremsstrahlung and pair production. I. Differential cross section, Phys. Rev. **93**, 768 (1954).
- [44] M. A. Kumakhov, On the theory of electromagnetic radiation of charged particles in a crystal, Phys. Lett. **57A**, 17 (1976).